JOC Article

Compared Behavior of 5-Deoxy-5-iodo-D-xylo- and L-Arabinofuranosides in the Reductive Elimination Reaction: A Strong Dependence on Structural Parameters and on the Presence of Zn^{2+}. A Combined Experimental and Theoretical Investigation

Eric Henon,*,† Ariane Bercier,‡ Richard Plantier-Royon,‡ Dominique Harakat,‡ and Charles Portella*,‡

Groupe de Spectrométrie Moléculaire et Atmosphérique (GSMA), UMR CNRS 6089 and Réactions Sélectives et Applications (RSA), UMR CNRS 6519, U.F.R Sciences, Université de Reims Champagne-Ardenne, Moulin de la housse, B.P. 1039, 51687 Reims Cedex 2, France

eric.henon@univ-reims.fr; charles.portella@univ-reims.fr

Received July 13, 2006

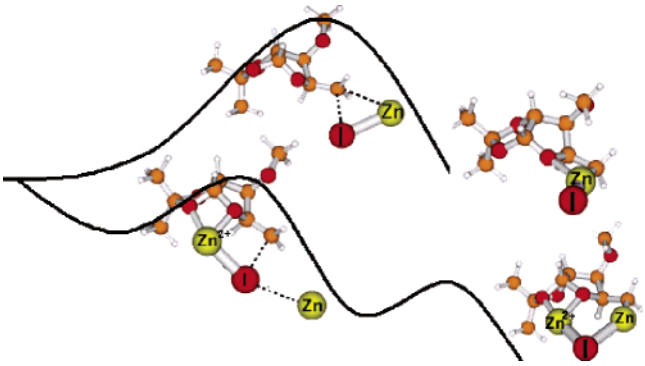

In the framework of a project devoted to the chemical transformation of monosaccharides from hemicelluloses into higher added value materials, the zinc-induced reductive elimination from 5-deoxy-5-iodo derivatives of D-xylose and L-arabinose was carried out. This study gave us the opportunity to observe surprising behaviors. In particular, the reaction strongly depends on structural parameters (protecting group pattern, configuration at C-4) and on the presence of Zn^{2+} ions. Collaterally with the experimental work, water solvent PCM HF-DFT (MPW1K/LANL2DZ) computations were performed to obtain insight into the mechanism for the reductive part of the reaction sequence. Without Zn^{2+}, the zinc insertion reaction was found to proceed through a concerted but non-synchronous process involving a relatively large energy barrier (32 kcal mol^{-1}) that directly leads to the presumed organozinc intermediate. In the presence of Zn^{2+}, a three-step mechanism was identified in which the cation coordinates the anomeric and ring oxygen atoms and also the sugar iodine atom, causing an activating effect on the zinc insertion process by facilitating the homolytic rupture of the C−I bond. Complexes between zinc and Zn^{2+} bound carbohydrates were characterized with large stabilization energies, suggesting that Zn^{2+} might enhance the affinity of the organic compound with the zinc metal surface.

Introduction

The reductive elimination from halogeno sugars (Bernet−Vasella reaction) is a reaction sequence frequently used in carbohydrate chemistry. First reported by Vasella's group with 6-deoxy-6-bromo-D-glucopyranose derivatives,[1] the method was extended to 5-deoxy-5-halo-pentofuranosides (Scheme 1).[2]

SCHEME 1

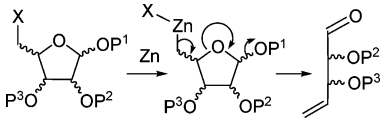

The metal that is by far the most used to induce this reaction is zinc, even if other reducing systems such as indium[3] and Zn/

* Corresponding authors. Tel.: (E.H.) 33 (0)326918774; (C.P.) 33(0)326913234.
† Groupe de Spectrométrie Moléculaire et Atmosphérique.
‡ Réactions Sélectives et Applications.

(1) Bernet, B.; Vasella, A. *Helv. Chim. Acta.* **1979**, *62*, 1990.

10.1021/jo0614590 CCC: $37.00
Published on Web 03/09/2007

Ag on graphite[4] gave good results. Zinc (powder or dust) needs to be activated (acidic washing, addition of TMSCl), and a protic medium such as an alcohol or THF containing between 3 and 15% of water is generally required to perform these reactions.[1] In the framework of a project dedicated to the chemical transformation of monosaccharides from hemicelluloses into higher added value materials, we considered the possibility to apply the reductive elimination methodology to 5-deoxy-5-iodo derivatives of D-xylose and L-arabinose, the main components of wheat hemicelluloses. This study gave us the opportunity to observe surprising behaviors. In particular, 5-deoxy-5-iodo-D-xylofuranosides can react quantitatively or can be perfectly inert, depending on the protecting group pattern. On the other hand, the epimeric L-arabino analogue of the unreactive D-xylo derivative proved to be quantitatively transformed under the same conditions. These experiments disclosed that the outcome of the Vasella reaction of 5-iodo-pentofuranosides depends strongly on structural parameters and prompted us to study more deeply the structure−reactivity relationship, in connection with the reaction conditions. A computational approach helped us to discriminate some hypotheses and to propose a mechanism for the reductive part of the reaction sequence. We report in this paper the results of this investigation.

Results and Discussion

Experimental Approach. Compounds **1x** and **1a**, obtained in five steps from D-xylose and L-arabinose, respectively,[5] were treated by acid activated zinc dust, under sonication, in a mixture of THF/H_2O 4:1, according to the conditions used by Madsen et al.[3a,6a] The results are summarized in Scheme 2. D-Xylose-derived iodo sugar **1x** proved to be perfectly inert, whereas the L-arabinose-derived analogue **1a** was completely converted into the expected aldehyde **2**, which was trapped in situ by *O*-benzylhydroxylamine to give **3** in 78% overall yield.

Since alkyl D-xylofuranoside analogues were reported to react under such conditions, the first step, the insertion of zinc into the C−I bond,[7] seems to depend on the C-4 configuration and/or on the rigidity of the fused bicyclic system.[6] To estimate these two parameters, both acetonides **1x** and **1a** were converted into the corresponding methylfuranosides **4x** and **4a**[5] by treatment in methanol under hydrogen chloride catalysis, and the methyl glycosides were then treated with zinc dust under the same conditions (Scheme 3). The two compounds behaved similarly: **4x** (mixture of anomers) or an equimolar mixture of epimeric iodo-methylfuranosides **4x** and **4a** were completely converted into the expected aldehyde **2** isolated as the *O*-benzyloxime **3** in 83 and 88% overall yield, respectively.[8]

SCHEME 2

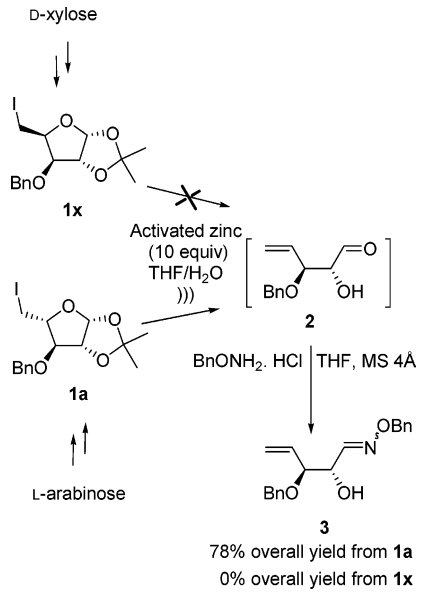

SCHEME 3

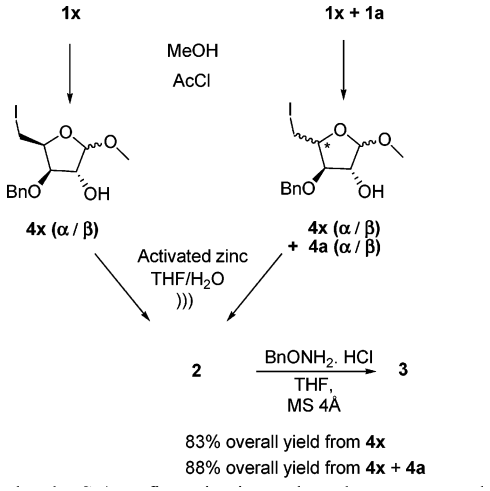

According to these results, the C-4 configuration is not the only parameter to be considered to explain the difference of reactivity between **1x** and **1a**: the overall shape of the molecule being of importance, as one could expect for a transformation of which the first step is a heterogeneous process. These observations led us to consider more deeply the reaction mechanism in connection with the reaction conditions.

To assess the influence of zinc treatment, the iodo derivatives **4x**, **1a**, and **1x** were treated with zinc dust under various conditions (Table 1). Compound **4x** was first considered as a model substrate. In all experiments, 10 equiv of zinc dust was used under ultrasound irradiation. While a total conversion of **4x** took place using acid washed zinc dust (entry 1), the starting material was completely recovered after sonication for 6 h using unactivated metal (entry 2).

(2) (a) Kobori, Y.; Myles, D. C.; Whitesides, G. M. *J. Org. Chem.* **1992**, *57*, 5899. (b) Uenishi, J.; Ohmiya, H. *Tetrahedron* **2003**, *59*, 7011.

(3) (a) Hyldtoft, L.; Madsen, R. J. *Am. Chem. Soc.* **2000**, *122*, 8444. (b) Yadav, J. S.; Reddy, B. V. S.; Srinivasa Reddy, K. *Tetrahedron* **2003**, *59*, 5333.

(4) (a) Fürstner, A.; Weidmann, H. *J. Org. Chem.* **1989**, *54*, 2307. (b) Fürstner, A.; Weidmann, H. *J. Org. Chem.* **1990**, *55*, 1363. (c) Fürstner, A. *Tetrahedron Lett.* **1990**, *31*, 3735. (d) Fürstner, A.; Jumbam, D.; Teslic, J.; Weidmann, H. *J. Org. Chem.* **1991**, *56*, 2213.

(5) Bercier, A.; Plantier-Royon, R.; Portella, C. *Green Chem.* **2006**, submitted.

(6) (a) Poulsen, C. S.; Madsen, R. *J. Org. Chem.* **2002**, *67*, 4441. (b) Boyer, F.-D.; Hanna, I.; Ricard, L. *Org. Lett.* **2001**, *3*, 3095.

(7) In carbohydrate chemistry, the zinc-induced ring opening reaction of halogeno sugars is generally referred to as a reductive elimination promoted by zinc; as pointed out by a referee, the insertion of a metal into a covalent bond can also be described as an oxidative addition of zinc to the C−I bond in the standard organometallic nomenclature.

(8) No difference of reactivity was observed between the two anomers of methylfuranoside **4x**. Ratio β/α remained constant (1.54) during the reaction.

TABLE 1. Influence of Reaction Conditions on the Ring Opening of 4x, 1a, and 1x

entry	substrate	reaction conditions	conversion[a]
1	**4x**	activated Zn dust THF/H_2O 4:1	Y
2	**4x**	untreated Zn dust THF/H_2O 4:1	N
3	**4x**	untreated Zn dust THF/H_2O 4:1 $ZnCl_2$ (1 equiv)	Y
4	**4x**	untreated Zn dust THF $ZnCl_2$ (1 equiv)	N
5	**1a**	untreated Zn dust THF/H_2O 4:1	N
6	**1a**	activated Zn dust THF/H_2O 4:1	Y
7	**1a**	untreated Zn dust THF/H_2O 4:1 $ZnCl_2$ (1 equiv)	Y
8	**1x**	activated Zn dust THF/H_2O 4:1	N
9	**1x**	untreated Zn dust THF/H_2O 4:1	N
10	**1x**	untreated Zn dust THF/H_2O 4:1 $ZnCl_2$ (1 equiv)	N

[a] N = no reaction. Y = conversion into enal **2**.

According to Luche,[9] the activation accomplished by ultrasound does not require, in most cases, a pre-activation of the metal before addition of the organic co-reagents. Hence, in the studied Vasella fragmentation, the role of the acidic treatment is not a simple activation of the zinc surface with elimination of zinc oxide. The HCl treatment induces the formation of zinc chloride at the metal surface. Such a Lewis acid could interact with the sugar derivative and participate in the overall activation process. Indeed, the addition of zinc chloride (1 equiv) to untreated zinc dust allowed a complete conversion of **4x** into the expected aldehyde **2** within 1.5 h under sonication (entry 3). This is exemplified by mass spectrometric monitoring of the reaction (Figure 1), which clearly exhibits the activating role of $ZnCl_2$. Actually, while the starting material remained inert under sonication using untreated zinc, a strong peak appeared ($m/z = 435$) in the spectrum after addition of $ZnCl_2$ that corresponds to a dimeric form of the hydroxy aldehyde **2** (the minor peak $m/z = 261$ is related to the C−I bond reduction compound).

Moreover, it can be noticed that the presence of water in the reaction medium is necessary since no reaction was observed in anhydrous THF (entry 4). These experiments show for the first time, in the Vasella fragmentation, the crucial role of zinc(II) previously formed at the metal surface during acidic washing. In the same way, we have checked that the reductive elimination reaction of the L-arabinose-derived acetonide **1a** was also controlled by acidic washing of zinc metal or by zinc chloride addition (entries 5−7). In contrast, the D-xylose-derived acetonide **1x** failed to react with whatever the reaction conditions (entries 8−10). Could the nature of the interaction between iodo sugar and Zn^{2+} ions explain the lack of reactivity of compound **1x** (as opposed to the reacting species **1a** and **4x**)? Following these experimental studies, a fundamental interest appeared for the understanding of the factors that influence the selectivity of the reaction and the role of Zn^{2+} in the Vasella reaction. Therefore, in parallel with the experimental work, we performed DFT molecular orbital computations to obtain an insight into the mechanism of the zinc insertion reaction.

Theoretical Considerations. To the best of our knowledge, there are no computational studies of the zinc-induced ring opening of iodo sugars. As suggested by Grob et al.,[11] the organozinc intermediate might be formed in the first step. Next, the cleavage of the molecule can proceed by three basic mechanisms differing in the order in which the fragments are released through a one- or a two-step process. For the concerted fragmentation, Grob[12] has derived rules according to which an antiperiplanar arrangement of the bonds that will be broken is required. Such stereoelectronically controlled fragmentations have been the subject of experimental[13] and computational[14,15] studies. It has been shown that the reduction of the carbon−halogen bond competes in some cases[4d] with the ring opening reaction. This can be taken as an indication of the existence of the organozinc intermediate. As explained before, the studied L-arabinose and D-xylose-derived iodo compounds behave quite differently in their reaction with zinc: they undergo either a ring opening Grob-type elimination or they are completely unreactive. It is to be noticed that no reduction products were formed in the latter case. The possibility that the acetal opens first (before the elimination) was ruled out. Actually, although this reaction could be promoted by Lewis acidic Zn^{2+}, **1x** remains intact in the presence of Zn^{2+} (Table 1, entry 10). Thus, it appears from our experimental results that the rate-limiting step for the studied molecules is the insertion reaction of zinc into the C−I bond. That is the reason why the subsequent fragmentation step was not modeled and why the possible organized aggregation of the RZnI species was not examined as well. We know of only one theoretical study in which the insertion reaction of zinc into the C−I bond has been examined. In this work,[16] the B3LYP/PVTZ//B3LYP/6-311G** barrier height computed within the gas-phase model for the insertion reaction of Zn into the C−I bond of CH_2I_2 was 29.5 kcal mol^{-1}. Moreover, our experimental results have shown that the use of zinc chloride is required to obtain the fragmentation products. Some Zn(II) promoted reactions are known in the literature.[17−20] For instance, complexation with Lewis acids is known to play a role in the radical conformation control in free radical reactions.[18] The presence of Zn^{2+} in the Vasella elimination of bromo derivatives obtained from D-glucose allowed the authors[19] to explain a subsequent rearrangement according to the chelation of the Lewis acid with the OH and carbonyl oxygens in the enal intermediate. Thus, our main objective in this theoretical study has been to contribute to the understanding of the role of the Lewis acid Zn^{2+} in the mechanism of the organozinc formation and to try to rationalize the observed reactivities.

(9) Luche, J.-L.; Sarandeses, L. A. In *Organozinc Reagents*; Knochel, P., Jones, P., Harwood, L. M.; Moody, C. J., Eds.; Oxford University Press Inc.: New York, 1999; pp 307−323.

(10) After sonication for 1 h and 30 min, **4x** totally disappeared, and aldehyde **2** was observed as a dimer using mass spectrometry ($m/z = 435 = [2 \times \mathbf{2} + Na]^+$).

(11) Grob, A.; Schiess, P. W. *Angew. Chem., Int. Ed. Engl.* **1967**, *6*, 1.

(12) Grob, A. *Angew. Chem., Int. Ed. Engl.* **1969**, *8*, 535.

(13) Bernet, B.; Vasella, A. *Helv. Chim. Acta* **1984**, *67*, 1328.

(14) Andrés, J.; Queralt, J. J.; Safont, V. S. *J. Phys. Org. Chem.* **1996**, *9*, 371.

(15) Queralt, J. J.; Andrés, J.; Moisés Canle, L.; Hermogenes Cobas, J.; Santaballa, J. A.; Sambrano, J. R. *Chem. Phys.* **2002**, *280*, 1.

(16) Fang, W.-H.; Phillips, D. L.; Wang, D.-q.; Li, Y.-L. *J. Org. Chem.* **2002**, *67*, 154.

(17) Nakamura, E.; Hirai, A.; Nakamura, M. *J. Am. Chem. Soc.* **1998**, *120*, 5844.

(18) Renaud, P.; Gerster, M. *Angew. Chem., Int. Ed.* **1998**, *37*, 2562.

(19) Holt, D. J.; Barker, W. D.; Ghosh, S.; Jenkins, P. R. *Org. Biomol. Chem.* **2004**, *2*, 1093.

(20) Yamamoto, H.; Futatsugi, K. *Angew. Chem., Int. Ed.* **2004**, *44*, 1924.

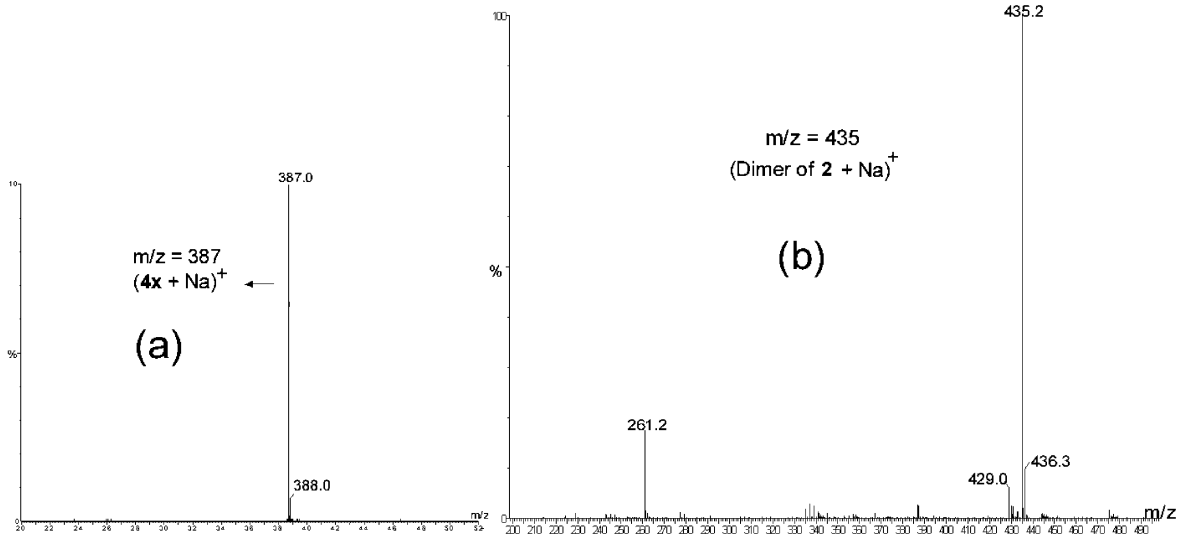

FIGURE 1. Mass spectrometry monitoring of the reductive elimination of **4x**: (a) with untreated zinc; THF/H_2O, sonication for 6 h and (b) addition of $ZnCl_2$; sonication for 1 h and 30 min.[10]

Reaction pathways were explored on the potential energy surface for both 1,2-*O*-isopropylidene L-arabino- and D-xylofuranose compounds. Solvent effects were assessed by the water solvent polarized continuum model (PCM). Full PCM geometry optimization calculations were performed for estimating the solvent effects on structures and the changes in energy for the zinc insertion reaction. As the reactions described herein were carried out in a polar solvent (water was added), the Zn^{2+} bound sugar species were assumed to be dissociated from the counterions because their charges are partially screened out by the solvent. The study of the solvent-separated complex between the Zn^{2+} bound sugar and the counterions would require simulations with explicit water molecules, which is more computationally expensive. One of the limitations of the present calculations is the simulation of an isolated Zn(0) atom. Metal zinc bulk could be further investigated by means of cluster models or the periodic slab[21] approach. Consequently, the structures and energy profile determined here with a continuum solvent model represent the first step toward a description of the metal zinc insertion reaction into the C−I bond in presence of Zn^{2+}. For reasons of computational cost, the calculations reported in the present work were performed on a model system obtained by replacing the benzyl group with the methyl group. The **x** and **a** notations have been reserved for the results concerning the structures derived from D-xylose and L-arabinose, respectively. **TSij** stands for the transition state connecting species **i** and **j**. Although a partial charge appears on the zinc metal and ion in the studied systems, these atoms are still designated as Zn and Zn^{2+} in the next part of the discussion according to their initial charge.

Zinc Insertion Reaction without Zn^{2+}. The insertion reaction without Zn^{2+} was found to occur through a concerted mechanism that directly leads to the organozinc intermediate. This result agrees favorably with the one-step insertion mechanism predicted by Fang et al.[16] for the insertion of Zn into the C−I bond of CH_2I_2. The solvent-optimized geometries of both reactants and transition states (TS) are shown in Figure 2, where relevant geometrical parameters have been indicated.

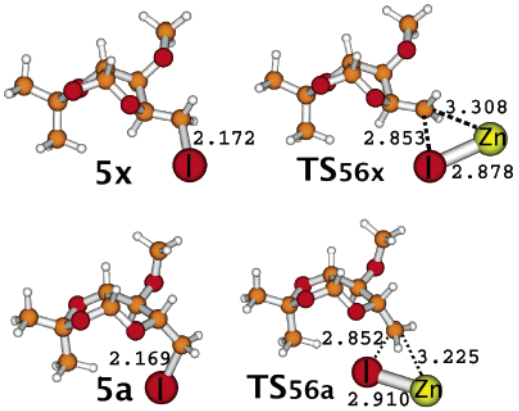

FIGURE 2. Reactants and transition state HF-DFT(MPW1K/LANL2DZ) optimized structures involved in the zinc insertion reaction via a concerted mechanism (distances in angstroms; **TS56** stands for the transition state connecting **5** and **6**). Geometries were fully optimized within the water PCM model.

In both cases (**TS56x** and **TS56a**), the incoming zinc atom approaches the carbon site from the opposite direction to the rest of the sugar. No transition state for the insertion reaction was found with the zinc atom placed near the oxygen atom of the ring. While the insertion process is concerted, it is non-synchronous with two important events taking place in transition state **TS56**. The first event is the C−I bond cleavage and the Zn−I bond formation. Actually, the breaking C−I bond (2.85 Å) in the transition state is significantly longer (by about 31%) than that in the unperturbed iodo sugar (2.17 Å), and the forming Zn−I bond length (2.83−2.87 Å) is only slightly different (by 12%) from the final bond length (2.56−2.59 Å) in the organozinc intermediate. The second event is the C−Zn bond formation (length of the forming C−Zn bond is 3.2−3.3 Å in **TS56** and 2.02 Å in the organozinc intermediate). This predicted non-synchronous behavior of the insertion process is consistent with the computed electron spin density distribution in the transition state, mainly localized on the carbon and zinc atoms (but not on the iodine atom). A summary of the potential energy profiles is shown in Figure 3. The PCM zero-point corrected relative energies are given with respect to the considered

(21) Bocquet, M-L.; Michaelides, A.; Loffreda, D.; Sautet, P.; Alavi, A.; King, D. A. *J. Am. Chem. Soc.* **2003**, *125*, 5620.

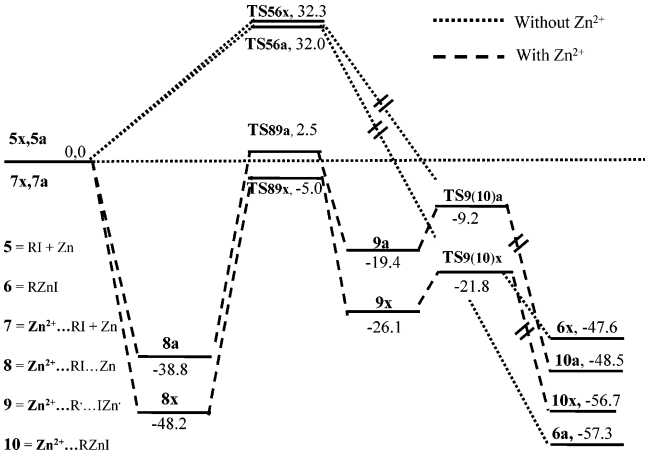

FIGURE 3. Water PCM HF-DFT(MPW1K/LANL2DZ) potential energy profiles for the zinc insertion reaction (with and without Zn^{2+}), including zero-point vibrational energy. **x** and **a** designate species derived from D-xylose and L-arabinose, respectively. Energies are in kcal mol^{-1}.

reactants (with or without Zn^{2+}). The insertion process was found to be exothermic by about 48−57 kcal mol^{-1}. The computed barriers are 32.3 and 32.0 kcal mol^{-1} (33.3 and 32.6 kcal mol^{-1} in the gas-phase model) above the reactants for **TS56x** and **TS56a**, respectively, in compliance with the barrier of 29.5 kcal mol^{-1} predicted by Fang et al.[16] at the gas-phase B3LYP/6-311G** level of theory for the insertion reaction of Zn into the C−I bond of CH_2I_2. These very close activation energies are, however, clearly inconsistent with the difference in reactivity observed between the L-arabinose and the D-xylose-derived iodo compounds in their reaction with zinc.

Geometries (Figure S1) and energy profiles (Figure S2) obtained in the gas phase are reported in the Supporting Information. From these results, it appears that the nonspecific solvent effect is small for the concerted mechanism.

Zinc Insertion Reaction with Zn^{2+}. As the Lewis acid Zn^{2+} has been experimentally found to play a role in the zinc-induced Vasella reaction mechanism, we examined how the presence of one Zn^{2+} ion could affect the structure and energy of the stationary points presented previously for the insertion step. The complexation of Zn^{2+} in the sugar was assumed to take place in the vicinity of the C−I bond. More precisely, the mode of bonding of Zn^{2+} with the studied iodo sugars was chosen according to the previously mentioned factors that seem to influence the reactivity. Hence, we envisaged the chelation of Zn^{2+} by the anomeric and ring oxygen atoms as depicted in structures **7x** and **7a** (Figure 4).

These two similar complexes involve three chelating atoms, including the iodine atom and resulting in a large stabilization energy of −98.2 and −112.5 kcal mol^{-1} (−212.4 and −226.9 kcal mol^{-1} in the gas phase), respectively. As a consequence, the C−I bond in the reactant is lengthened by approximately 0.03−0.05 Å when Zn^{2+} coordinates with the organic compound, thus favoring a possible cleavage. Unlike the previous concerted two-stage reaction,[22] in the presence of Zn^{2+}, the zinc insertion was found to proceed through a three-step process. Actually, no indication for the occurrence of a direct reaction, characterized by a single barrier between the reactants and the

(22) Dewar, J. S.; Olivella, S.; Stewart, J. J. P. *J. Am. Chem. Soc.* **1986**, *108*, 5771.

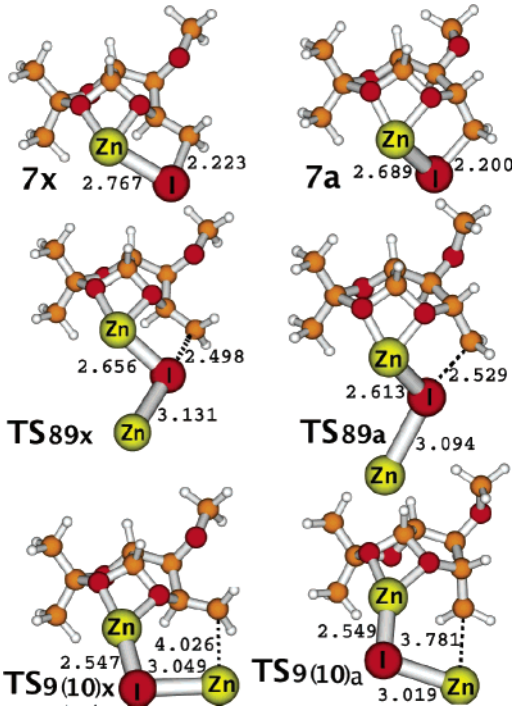

FIGURE 4. Zn^{2+} bound reactants and transition state HF-DFT-(MPW1K/LANL2DZ) optimized structures involved in the zinc insertion reaction through an indirect mechanism (distances in angstroms; **TSij** stands for the transition state connecting **i** and **j**). Geometries were fully optimized within the water PCM model.

product, could be found by our computations. Instead, two intermediates (referred to as **8** and **9**) were identified and confirmed to be connected with the reactants, TSs, and products according to the reaction scheme

$$Zn^{2+}\cdots RI\ (\mathbf{7}) + Zn \rightarrow Zn^{2+}\cdots RI\cdots Zn\ (\mathbf{8}) \rightarrow \mathbf{TS89} \rightarrow Zn^{2+}\cdots R^{\bullet}\cdots IZn^{\bullet}\ (\mathbf{9}) \rightarrow \mathbf{TS9}\ (\mathbf{10}) \rightarrow Zn^{2+}\cdots RZnI\ (\mathbf{10})$$

Selected optimized geometries involved in this mechanism are presented in Figures 4 and 5.

In this mechanism, after the coordinate Zn^{2+} intermediate **8** is formed (step 1), the insertion reaction starts via the transition state **TS89**, which describes (step 2) both the homolytic rupture of the C−I bond and the Zn−I bond formation. This concerted process leads to the intermediate **9**, the equilibrium structure of which is described in Figure 5. Interestingly, the two unpaired electrons of **9** are mainly located on the carbon atom (1.1) and the zinc atom (0.9), thus facilitating the formation of a C−Zn bond to produce the organozinc intermediate. From an entropy point of view, it should be noted that the cation−halogen bond interaction in **9** keeps the newly formed $IZn^{\bullet}$ fragment close to the region of the sugar after the dissociation, in particular, near the carbon radical center. This also facilitates the next association step. Step 3 is the association of the two fragments through the transition structure **TS9** (**10**).

For the discussion, we will first focus on the influence of Zn^{2+} on the insertion process (**TS89** and **TS9** (**10**)). The role of the precursor intermediate **8** is addressed at the end of the discussion.

In comparison with **TS56**, the relative energies of **TS89** and **TS9** (**10**) lie near and below the reactant levels, respectively

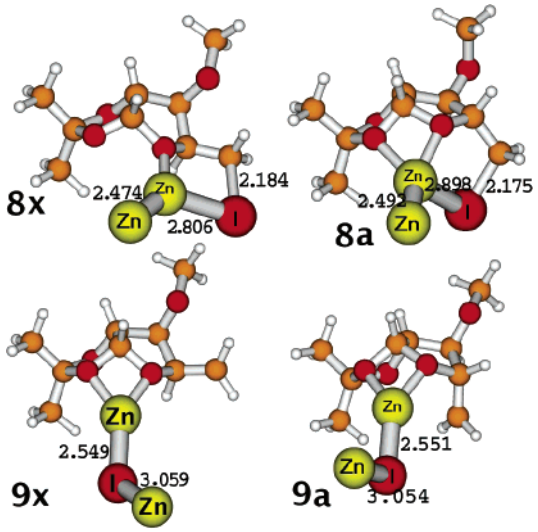

FIGURE 5. HF-DFT(MPW1K/LANL2DZ) optimized structures of intermediates involved in the zinc + Zn^{2+} bound sugar reaction system (distances in angstroms). Geometries were fully optimized within the water PCM model.

(Figure 3). Interestingly, step 2 is concerted but non-synchronous. Actually, according to the small degree of C−I bond lengthening in the transition state **TS89** (12−15%), there is no doubt that the C−I bond breaking takes place only in the second half of step 2 between **TS89** and **9**. Thus, in contrast with **TS56**, the reaction energy begins to fall in step 2 before the bond cleavage is fully developed. Part of the reason is that the C−I bond cleavage allows for the beneficial strengthening of the $Zn^{2+}\cdots$I coordinate bond (2.77−2.69 Å in **7x** and **7a** and 2.55 Å in **9x** and **9a**). So, it appears that the presence of Zn^{2+} causes the C−I bond to be weakened and facilitates its dissociation. On the other side, it is the Zn−I bond making that takes place in the first half of step 2 (the forming Zn−I bond length in **TS89** is only slightly different by 1−2% from its final value in **9**). However, for this bond to be formed, the Zn$\cdots Zn^{2+}$ coordinate bond in **8** must be cleaved, resulting in a large energy barrier for step 2 (41−43 kcal mol^{-1}). Actually, due to the proximity of the two zinc atoms in **TS89**, the minimum energy pathway (Figure 3) has been found to connect **TS89** to the stable Zn$\cdots Zn^{2+}$ coordinated complex **8** in the reverse direction (further information is given in the Experimental Section). Thus, a chemically activated intermediate **8** can be formed from **7** in a barrier-less association between Zn^{2+} bound sugar and zinc atom. However, owing to the large stabilization potential energy (39−48 kcal mol^{-1}) of **8**, it is likely that this intermediate species be stabilized by energy transfer to the solvent precluding the insertion reaction of the zinc metal atom coordinated to the Zn^{2+} center. Hence, it is not unreasonable to assume that the coordination interaction (between Zn^{2+} and Zn) first governs the chemisorption of the Zn^{2+} bound substrate on the metal surface. Nevertheless, this does not rule out a subsequent insertion mechanism involving another reacting zinc metal atom. It then would be interesting to study the effect of the presence of more than a single zinc metal atom on the previously presented indirect mechanism. More precisely, one may wonder if a Zn decoordinationless mechanism could exist for the zinc insertion process starting from the chemisorbed precursor that would involve an activation energy lower than the large **8**-**TS89** barrier. Our gas-phase results suggest the possible existence of such a mechanism (discussed hereafter). At this stage, it is worth noting that species **8x** and **8a** slightly differ in structure. Both involve the Zn$\cdots Zn^{2+}$ coordinate bound associated with a rather large stabilization energy, but the former is tri-coordinated while the latter is tetra-coordinated. This might support the idea that the reaction selectivity experimentally observed in the Vasella reaction of the D-xylose-derived acetonide **1x** and the L-arabinose-derived acetonide **1a** could originate from the behavior of the corresponding Zn^{2+} bound carbohydrates at the metal surface.

Comparison with the gas-phase results (reported in the Supporting Information) indicates that the nonspecific interaction of the solvent exerts only a small effect on both the energetic and the geometrical parameters. The main characteristics of the gas-phase profile remain valid in solution except for **TS89x**, which in the gas phase (Figure S3) does not involve any decoordination during the Zn−I bond making/C−I bond breaking process. Indeed, the location of the zinc atom in **TS89x** changes significantly without solvent effect (the ZnIZn bond angles in the solvent and gas phase are 94.2 and 155.6°, respectively). As a consequence, the gas-phase minimum energy pathway (Figure S2) connects **TS89x** to the relatively loosely bound tri-coordinated complex **8′x** in the reverse direction. In this intermediate complex, the zinc atom is not strongly bound to Zn^{2+} but interacts with the iodine atom with a stabilization energy of only −10.6 kcal mol^{-1}. The **8′x** → **TS89x** barrier height is then predicted to be much lower (9.6 kcal mol^{-1}) than the one (36−43 kcal mol^{-1}) required to break the Zn$\cdots Zn^{2+}$ coordination bond. These gas-phase results emphasize the Zn^{2+} assistance for the insertion process when no decoordination is required. A Zn$\cdots Zn^{2+}$ complex **8x** (Figure S4, analogue to **8x** in Figure 5) was also found in the gas-phase model with a stabilization energy of −44.6 kcal mol^{-1}, but it is not directly connected to the C−I dissociation pathway in this case.

It results from our calculations that the coordinate bond between Zn^{2+} and iodine atom in the parent carbohydrate can play a substantial role in lowering the activation energy for the insertion process. Such a bond was also found at the gas-phase level of theory in the Zn^{2+} bound methylfuranosides (α/β) derived from **7x** and **7a** (noted **11x**α, **11x**β, **11a**α, and **11a**β in the Supporting Information), indicating that these compounds may also be influenced by the presence of Zn^{2+} in their reaction with metal zinc as suggested by our experimental findings. Obviously, further theoretical work, especially on the organic molecule at the zinc surface, is required before a deeper understanding can be gained in the reactivity difference observed between the two sugars. Actually, the investigated processes occur most certainly on the surface of the bulk metal, involving the zinc−organic species. It should be mentioned that in employing the zinc/silver−graphite reagent, Fürstner et al.[4d] achieved the reduction of the C−I bond from the iodo sugar **1x** (which failed to react in our case).

Conclusion

Experimental evidence shows that the zinc-induced reductive elimination of 5-deoxy-5-iodo-pentofuranosides is strongly dependent on both structural parameters and reaction conditions. The result is clearly a function of the nature of the protecting group and of the configuration at C-4 as well. At the same time, experiments clearly show that the reaction is very sensitive to the presence of the Zn(II) Lewis acid. Our theoretical investigation gives new hints to explain the role of Zn^{2+}, assuming that the fragmentable substrate is the organozinc compound. From

our calculations, we find that, in the presence of Zn^{2+}, the insertion reaction takes place in three elementary steps with transition states near or below the reactant energy level. The cation is likely to coordinate the anomeric and ring oxygen atoms and also the halogen of the sugar, causing an activating effect on the zinc insertion process by facilitating the homolytic rupture of the C−I bond. The dissociation is followed by an association step via a loose transition state. The whole process starts off with the barrier-less formation of a complex between zinc and Zn^{2+} bound sugar involving a $Zn\cdots Zn^{2+}$ coordinate bond in the iodo sugar. No significant difference was found that could explain the opposite reactivity displayed by the two iodo sugars. It turns out that the $Zn\cdots Zn^{2+}$ interaction results in a large stabilization energy, suggesting that Zn^{2+} might enhance the affinity of the organic compound with the zinc metal surface whatever the considered sugar in our case. Despite our theoretical work, we have to conclude that the mechanism for the zinc insertion reaction into the C−I bond of the iodo sugars derived from D-xylose and L-arabinose is not satisfactorily known yet. For the final clarification of these hypotheses, the carbohydrate environment has to be taken into account. More precisely, it would be interesting to address the role of explicit water molecules and metal surface in the previously presented Zn^{2+} assisted mechanism.

Experimental Section

Acid Activation of Zinc. Zinc dust was stirred in a 3 N aqueous HCl solution (0.5 mL/mmol of zinc) for 5 min, then filtered, and washed with water (0.5 mL/mmol), ethanol (0.5 mL/mmol), and ether (0.5 mL/mmol). Finally, the material was dried under high vacuum with a heat gun until the powder became pale gray.

Reaction with Activated Zinc. To a solution of 5-iodo compounds in a 4:1 THF/H_2O mixture (5 mL/mmol) was added activated zinc dust (10 equiv). The reaction was sonicated at 40 °C until the starting material disappeared. The mixture was filtered through cotton to eliminate zinc, and solvents were evaporated.

Reaction with Untreated Zinc and $ZnCl_2$. To a solution of 5-iodo compounds in a 4:1 THF/H_2O mixture (5 mL/mmol) was added zinc dust (10 equiv). The reaction was sonicated at 40 °C for 6 h, then anhydrous $ZnCl_2$ (1 equiv) was added. The reaction was sonicated at 40 °C until the starting material disappeared.

Computational Details. Calculations were performed using the Gaussian 98 and Gaussian 03 packages.[23,24] The presence of two zinc atoms and one iodine atom along with the studied protected sugars made the use of high level theoretical methods costly. Hence, the calculations reported in the present work were performed on a model system obtained by replacing the benzyl group with the methyl group. Several levels of theory were tested previously to choose the HF−DFT MPW1K[25]/LANL2DZ[26−29] method. In particular, the standard HF/LANL2DZ or HF−DFT(B3LYP)/LANL2DZ methods did not allow for locating the transition state such as **TS89** or **TS9 (10)**. The MPW1K hybrid density functional was developed relatively recently by Truhlar and co-workers with the aim of being used in predicting chemical reactivity.[25] The reactivity of some organometallic complexes has suitably been obtained using the HF−DFT MPW1K/LANL2DZ methodology,[30] even though the use of a basis set larger than LANL2DZ is recommended. As the molecule investigated is relatively large, it was not possible to increase the size of the basis set in our case. Reactants, complexes, and transition state structures were fully optimized using the analytical gradients at the HF−DFT MPW1K/LANL2DZ level of theory within both the gas-phase model and the PCM.[31−33] In the latter case, the structures (minima and first-order saddle points) were fully optimized in the field of water using the solvent accessible surface (SAS). The standard dielectric constant of water implemented in the Gaussian program was employed ($\epsilon = 78.39$). Vibrational frequencies were determined within the harmonic approximation, at the same level of theory (vacuum and PCM). Small imaginary frequencies were observed for some stationary points at the PCM level of theory. This may originate in the approximate algorithm used to obtain the analytical PCM second derivatives. Thus, for these stationary points, the second derivatives were computed numerically using analytically calculated PCM first derivatives (this took 110 CPU hours each). Despite these precautions, one small imaginary frequency remained for species **9a** (32i). This low frequency is likely to be sensitive to the step size for the numerical differentiation in this flat region of the PES. Because of the computational cost of such numerical calculations, the gas-phase ZPE was used in this case. The energies presented in this work include the zero-point energy correction. Gas-phase entropies and Gibbs free energies were estimated at 298 K. All transition states were characterized by one imaginary frequency (first-order saddle points on the potential energy surface (PES)) associated with the desired reaction pathway. The unrestricted approach was used for transition states and biradical species. The resulting spin-contaminations in the unrestricted electronic structure calculations of **TS56x**, **TS56a**, **TS89x**, and **TS89a** were 0.72, 0.68, 0.29, and 0.39, respectively. The spin-contaminations of the HF−DFT wave functions for **TS9** (**10**)**x**, **TS9** (**10**)**a**, **9x**, and **9a** were in the range of 0.98−1.00. The quadratically convergent algorithm (much slower than DIIS) was used for the studied systems because SCF iterations sometimes had convergence difficulties. Some HF−DFT wave functions were first obtained with an internal instability for transition states and biradical species. That is the reason why the stability of the solution was tested for each stationary point before any geometry

(23) Frisch, M. J.; Trucks, G. W.; Schlegel, H. B.; Scuseria, G. E.; Robb, M. A.; Cheeseman, V. G.; Zakrzewski, J. R.; Montgomery, R. E.; Stratmann, J. C., Jr.; Burant, J. C.; Dapprich, S.; Millam, J. M.; Daniels, A. D.; Kudin, K. N.; Strain, M. C.; Farkas, O.; Tomasi, J.; Barone, V.; Cossi, M.; Cammi, R.; Mennucci, B.; Pomelli, C.; Adamo, C.; Clifford, S.; Ochterski, J.; Petersson, G. A.; Ayala, P. Y.; Cui, Q.; Morokuma, K.; Salvador, P.; Dannenberg, J. J.; Malick, D. K.; Rabuck, A. D.; Raghavachari, K.; Foresman, J. B.; Ciolowski, J.; Ortiz, J. V.; Baboul, A. G.; Stefanov, B. B.; Liu, G.; Liashenko, A.; Piskorz, P.; Komaromi, I.; Gomperts, R.; Martin, R. L.; Fox, D. J.; Keith, T.; Al-Laham, M. A.; Peng, C. Y.; Nanayakkara, A.; Challacombe, M.; Gill, P. M. W.; Johnson, B.; Chen, W.; Wong, M. W.; Andres, J. L.; Gonzalez, C.; Head-Gordon, M.; Replogle, E. S.; Pople, J. A. *Gaussian 98*, revision A.11.1; Gaussian, Inc.: Pittsburgh, PA, 2001.

(24) Frisch, M. J.; Trucks, G. W.; Schlegel, H. B.; Scuseria, G. E.; Robb, M. A.; Cheeseman, J. R.; Montgomery, J. A., Jr.; Vreven, T.; Kudin, K. N.; Burant, J. C.; Millam, J. M.; Iyengar, S. S.; Tomasi, J.; Barone, V.; Mennucci, B.; Cossi, M.; Scalmani, G.; Rega, N.; Petersson, G. A.; Nakatsuji, H.; Hada, M.; Ehara, M.; Toyota, K.; Fukuda, R.; Hasegawa, J.; Ishida, M.; Nakajima, T.; Honda, Y.; Kitao, O.; Nakai, H.; Klene, M.; Li, X.; Knox, J. E.; Hratchian, H. P.; Cross, J. B.; Bakken, V.; Adamo, C.; Jaramillo, J.; Gomperts, R.; Stratmann, R. E.; Yazyev, O.; Austin, A. J.; Cammi, R.; Pomelli, C.; Ochterski, J. W.; Ayala, P. Y.; Morokuma, K.; Voth, G. A.; Salvador, P.; Dannenberg, J. J.; Zakrzewski, V. G.; Dapprich, S.; Daniels, A. D.; Strain, M. C.; Farkas, O.; Malick, D. K.; Rabuck, A. D.; Raghavachari, K.; Foresman, J. B.; Ortiz, J. V.; Cui, Q.; Baboul, A. G.; Clifford, S.; Cioslowski, J.; Stefanov, B. B.; Liu, G.; Liashenko, A.; Piskorz, P.; Komaromi, I.; Martin, R. L.; Fox, D. J.; Keith, T.; Al-Laham, M. A.; Peng, C. Y.; Nanayakkara, A.; Challacombe, M.; Gill, P. M. W.; Johnson, B.; Chen, W.; Wong, M. W.; Gonzalez, C.; Pople, J. A. *Gaussian 03*, revision C.02; Gaussian, Inc.: Wallingford, CT, 2004.

(25) Lynch, B. J.; Fast, P. L.; Harris, M.; Truhlar, D. G. *J. Phys. Chem. A* **2000**, *104*, 4811.

(26) Dunning, T. H.; Hay, P. J. In *Modern Theoretical Chemistry*; Schaefer, H. F., III, Ed.; Plenum: New York, 1976; pp 1−28.

(27) Hay, P. J.; Wadt, W. R. *J. Chem. Phys.* **1985**, *82*, 270.

(28) Wadt, W. R.; Hay, P. J. *J. Chem. Phys.* **1985**, *82*, 284.

(29) Hay, P. J.; Wadt, W. R. *J. Chem. Phys.* **1985**, *82*, 299.

(30) Iron, M. A.; Lo, H. C.; Martin, J. M. L.; Keinan, E. *J. Am. Chem. Soc.* **2002**, *124*, 7041.

(31) Miertus, S.; Scrocco, E.; Tomasi, J. *Chem. Phys.* **1981**, *55*, 117.

(32) Cossi, M.; Scalmani, G.; Rega, N.; Barone, V. J. *Chem. Phys.* **2002**, *117*, 43.

(33) Cammi, R.; Mennucci, B.; Tomasi, J. *J. Phys. Chem. A* **2000**, *104*, 5631.

optimization or frequency calculation and why the wavefunction was reoptimized to the lower energy solution when an instability was found. Special care was taken to determine minimum energy pathways (MEPs), performing intrinsic reaction coordinate analyses (IRC) to confirm that a specific transition state connected to the designated local minima. Only gas-phase IRC calculations were carried out because the reaction path following was a time-consuming procedure. Some problems arose, however, during this procedure. For transition states **TS9** (**10**) (association pathway), the vibrational analysis gave a very low imaginary frequency (about 47i), whose animation is consistent with the formation of the C−Zn bond but through a very loose TS. This is the reason why the standard IRC algorithm failed at connecting **TS9** (**10**) to the corresponding minima, due to the flatness of the PES in this region. Rotational energy profiles for internal rotations about the $I-Zn^{2+}$ bond in species **9x** and **9a** were performed to estimate a possible rotational barrier before the reacting system **9** connected to **TS9** (**10**). The energy was found to increase by no more than 1 kcal mol^{-1} as the $Zn-I-Zn^{2+}-O$ dihedral angle was scanned from its value in **9** to its value in **TS9** (**10**). In other respects, the IRC calculation from **TS89a** in the reverse direction terminated after 185 steps (of 0.06 $amu^{1/2}$) before reaching the complex **8a** but had progressed sufficiently in this direction to establish the C−I dissociation pathway. The last IRC point (denoted **8′a** in the following discussion) energy lies only 3.0 kcal mol^{-1} below the reactant level with small energy gradients (but nonzero), and the corresponding geometry **8′a** is very similar to that of complex **8′x** (C−I = 2.257 Å and Zn−I = 3.455 Å in **8′a**, as compared to 2.238 and 3.427 Å in **8′x**). A straightforward geometry optimization of this **8′a** system led to the formation of the notably stable complex **8a** in which the zinc atom was strongly bound to Zn^{2+}. We have made a detailed search on the PES but have not been able to find a loosely bound complex **8′a** (located rigorously as a minimum) similar to **8′x** involving the Zn···I interaction. In particular, two relaxed potential energy scans were carried out starting from the geometrical parameters of **8′a**. First, the energy was observed to increase continuously as the Zn−I distance was scanned from 3.44 up to 5.0 Å while holding fixed the $Zn-I-Zn^{2+}$ coordinate to its value in **8′a** (103.0°). In the second scan, the representative point of the system on the PES moved down to the potential energy well of **8a** as the $Zn-I-Zn^{2+}$ coordinate was scanned from 122 to 50°.

Acknowledgment. C.R.I.H.A.N. computing center and the computational center of the Université de Reims Champagne-Ardenne (ROMEO) are acknowledged for the CPU time donated. The authors thank Prof. F. Bohr for helpful discussions. This work was supported by the Contrat de Plan Etat-Région (Program GLYCOVAL−Europol'agro). We are indebted to CNRS and Région Champagne-Ardenne for a PhD fellowship (A.B.).

Supporting Information Available: General methods; experimental procedures and characterization data (^1H and ^{13}C NMR spectra, electrospray ionization mass spectra) for compound **3**; and computational data: potential energy, zero point vibrational energy (in hartrees), Cartesian coordinates of all stationary points both in the gas phase and in the water PCM models. This material is available free of charge via the Internet at http://pubs.acs.org.

JO0614590